Journal of Alloys and Compounds 495 (2010) 565–569

Contents lists available at ScienceDirect

Journal of Alloys and Compounds

journal homepage: www.elsevier.com/locate/jallcom

Temperature effects on structural properties in the synthesis of nanocrystalline $Zr_{0.5}Ce_{0.5}O_2$ solid solution: A study by XRD and HRTEM

Rodolfo O. Fuentes[a,b,*], J. Derek Woollins[b], Richard T. Baker[b]

[a] CINSO (Centro de Investigaciones en Sólidos), CITEFA-CONICET, J.B. de La Salle 4397, 1603 Villa Martelli, Buenos Aires, Argentina
[b] School of Chemistry, University of St. Andrews, North Haugh, St. Andrews, Fife KY16 9ST, United Kingdom

ARTICLE INFO

Article history:
Received 16 July 2008
Received in revised form 16 October 2009
Accepted 28 October 2009
Available online 5 November 2009

Keywords:
Nanostructured materials
Zr–Ce mixed oxides
Chemical synthesis
X-ray diffraction
Transmission electron microscopy

ABSTRACT

In the present work, a nanostructured $Zr_{0.5}Ce_{0.5}O_2$ solid solution was synthesized using a citrate complexation technique with different thermal treatments. The resulting powders were characterized by employing X-ray diffraction (XRD) and high resolution transmission electron microscopy (HRTEM). A qualitative analysis of the XRD data indicated that all samples exhibited a tetragonal phase ($P4_2/nmc$ space group). In HRTEM observations, the internal crystal structure of the nanoparticles was studied and the primary particle sizes were measured. Average crystallite size, obtained from the XRD data using the Scherrer equation, ranged from 4.1 nm to 7.7 nm.

1. Introduction

ZrO_2–CeO_2 substitutional solid solutions have attracted particular interest in recent years due to their extensive use in different fields, for example, as active supports or "oxygen buffers" in three-way catalysts (which are applied in controlling the emissions of NO_x, CO and hydrocarbons from automotive exhausts) [1–3]. The properties of zirconia–ceria mixed oxides are strongly related to their crystal structure. In particular, the metastable forms of the tetragonal phase have been widely investigated since they are the most suitable for certain applications [4,5]. This wide use of these systems as catalyst components prompted a renewed interest with regards to these materials in the form of nanosized, high surface area powders. In particular, in the catalytic converter, CeO_2 is present as a mixed oxide with ZrO_2. Without the addition of zirconia, ceria sinters rapidly in high temperature applications, losing surface area and catalytic activity. In contrast, CeO_2–ZrO_2 mixtures maintain their surface area and catalytic activity for many years under very harsh environments [6]. Such thermal stability would be advantageous in catalysts for applications in SOFC-related catalyst systems.

Several routes have previously been used for the synthesis of compositionally homogeneous nanocrystalline ceria-based solid solutions, including the sol–gel method [7], hydrothermal synthesis [8], the polymerized complex method [9], the amorphous citrate process [10] and gel-combustion [11]. Lamas et al. [12] reported a study of the tetragonal–cubic phase transition on nanocrystalline powders obtained by a pH-controlled nitrate-glycine gel-combustion method (average crystallite sizes were in the range of 8–20 nm). The tetragonal to cubic phase transition as a function of ceria content was found close to 85 mol% CeO_2. The ZrO_2–50 mol% CeO_2 solid solution exhibited the metastable t' form of tetragonal phase ($P4_2/mnc$ space group).

In a previous study, the ZrO_2–CeO_2 solid solution, synthesized by a citrate complexation technique, with 50 mol% CeO_2 was found to have the smallest crystallites (4.8 nm) and the highest BET specific surface area (SSA, 46 $m^2\,g^{-1}$) compared with other compositions synthesized by the same route [13]. For this reason, $Zr_{0.5}Ce_{0.5}O_2$ is a good candidate anode catalyst for intermediate-temperature (IT)-SOFCs.

In the present work, we report a structural characterization of a $Zr_{0.5}Ce_{0.5}O_2$ mixed oxide synthesized by a citrate complexation with different thermal treatments. The resulting powders were characterized by employing X-ray diffraction (XRD) and high resolution transmission electron microscopy (HRTEM).

2. Experimental procedure

$Zr_{0.5}Ce_{0.5}O_2$ (ZC) was synthesized from nitrate precursors by complexing the metal cations with the citrate ion. Cerium nitrate hexahydrate (99.99%, Aldrich) and zirconium dinitrate oxide (99.9%, Alfa Aesar) were employed as precursors. Each nitrate was dissolved in H_2O individually and then the solutions were mixed. Anhy-

* Corresponding author at: CINSO (Centro de Investigaciones en Sólidos), CITEFA-CONICET, J.B. de La Salle 4397, 1603 Villa Martelli, Buenos Aires, Argentina.
E-mail address: rfuentes@citefa.gov.ar (R.O. Fuentes).

0925-8388/$ – see front matter © 2009 Elsevier B.V. All rights reserved.
doi:10.1016/j.jallcom.2009.10.249

drous citric acid (99.5%, Riedel-deHaen) was dissolved in water and then was added to the cation solution. The molar ratio of total oxide (TO):citric acid (CA) was 1:2. After homogenization of this solution, the temperature was raised to 80 °C, and the solution maintained under stirring to remove excess water and to convert it to a transparent gel. While raising the temperature, the solution became more viscous with evolution of foam, and finally it gelled without any visible precipitation or turbidity. As the solution was maintained at this temperature, there was an increase in viscosity and simultaneous elimination of water and NO_2. The initial thermal decomposition of the precursor was carried out at 250 °C for 1 h. The resulting ash-like material was then pyrolyzed at different temperatures for 1 h. For identification purposes, samples received the denomination ZC250, ZC400, ZC600 and ZC800, where the number indicates the calcination temperature in °C.

Thermal analysis (TG/DTA) of gel precursors of ZC was carried out in flowing air with a heating rate of 5 °C/min up to 800 °C in a Pt crucible, using a TA Instruments SDT 2960. The residual carbon content of the samples after calcination at different temperatures in air was determined by elemental analysis using a Carlo Erba CHNS analyser.

XRD experiments were carried out using a Philips PW 1710 diffractometer (Cu Kα radiation). Data in the angular region of $2\theta = 20–100^\circ$ were collected at room temperature in a step-scanning mode, with a step length of 0.02° and a step-counting time of 12 s. High-grade silicon powder was used as a standard to allow for the instrument broadening correction.

Raman spectra were recorded using a Perkin Elmer 2000 (FT) spectrophotometer. A 1.064 nm Nd/YAG laser line was used as the excitation radiation and the laser power at the sample was 500 mW. Spectra acquisition consisted of 124 scans at 2 cm^{-1} resolution.

The SSA measurements were carried out using Brunauer, Emmett and Teller (BET) analysis by nitrogen adsorption (ASAP 2010, Micromeritics).

TEM images, elemental maps and selected area electron diffraction (SAED) patterns of the sample were obtained using a JEOL 2010 TEM instrument with a LaB_6 filament and equipped with a Gatan digital camera. Samples were prepared by dipping a 3 mm copper grid coated with holey carbon film into a dispersion of the sample powder in hexane.

3. Results and discussion

The TGA/DTA plot (carried out in air) for the ZC gel precursor is shown in Fig. 1. The DTA curve exhibits two large exothermic peaks, starting at 118 °C and 266 °C, respectively. The higher temperature peak can be related to the burn out of organic materials, with associated release of CO, CO_2 and NO_x, and to the crystallization of the ZC solid solution. A third small exothermic peak, starting at 164 °C can be observed, which could be due to the decomposition of the nitrate. Mass loss occurred in three steps according to the TGA curve, all of which are correlated with exothermic peaks observed in the DTA plot. Total mass loss up to 500 °C is about 74%.

The origin of the first large exothermic peak (118 °C), which is coincident with an abrupt mass loss observed in the TGA curve, is initially puzzling. In previous work [13], TGA/DSC studies were performed on very similar Ce–Zr mixed oxide gel precursors, employing O_2 as a carrier gas and with analysis of the off-gas using

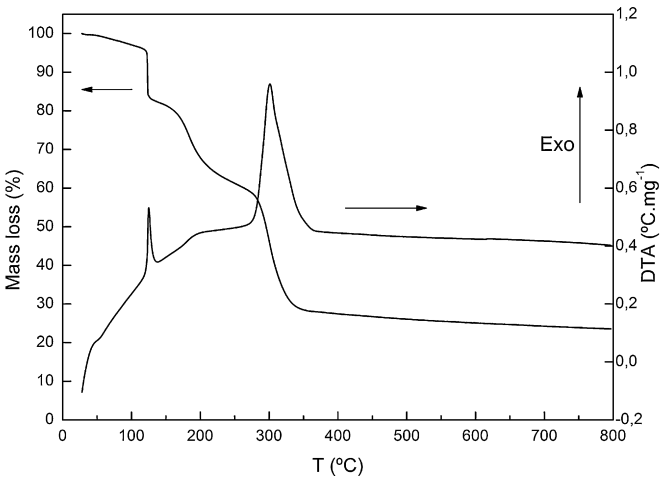

Fig. 1. TG/DTA curves of metal nitrate precursor mixture of ZC sample.

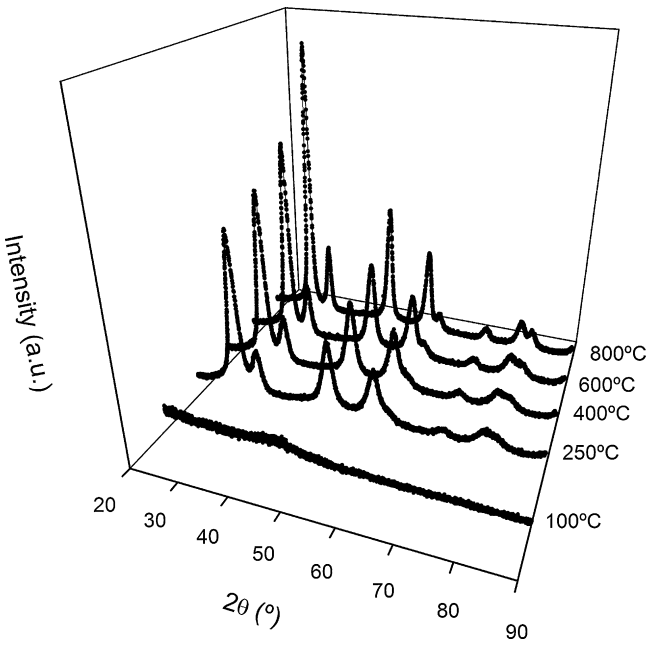

Fig. 2. XRD patterns for nanocrystalline ZC samples calcined at the temperatures indicated.

mass spectrometry (MS). The MS data showed that H_2O is the main product released in the first exothermic peak with only traces of NO_x. However, for simple H_2O evaporation an endothermic peak would be expected. In this context, this peak can be ascribed to the polymerisation reactions accompanying gel formation. In these reactions the Ce and Zr complex cations are increasingly cross-linked by the progressive substitution of water ligands by the tridentate citrate ion. Since the $-COO^-$ groups would be expected to bond more strongly than water to the metal centres and since the formation of a gel from a solution would cause an increase in entropy, this process is expected to be exothermic. Therefore, the low temperature peak in the TGA curve can be explained.

The carbon content of the ZC powders decreased with increasing calcination temperature. For example, samples calcined at 250 °C and 800 °C exhibit values of residual carbon content (%) of 0.79 and 0.17, respectively. In previous work, we found the carbon content was 0.35% at 500 °C [13]. Therefore it is clear that the carbon content in samples synthesized by this citrate complexation route is very low.

XRD patterns at room temperature for $Zr_{0.5}Ce_{0.5}O_2$ powders calcined at different temperatures are shown in Fig. 2. Powder calcined at 100 °C for 1 h shows an amorphous structure while the powders calcined at higher temperatures exhibited resolved, and relatively broad, peaks, ascribable to the presence of small crystallites in the samples. The average crystallite size, D_{XRD}, was determined using the Scherrer formula [14], $D = 0.9\lambda/\beta\cos\theta$, where λ is the wavelength of the radiation (1.54056 Å), β is the corrected peak width at half-maximum intensity (FWHM in radians), and θ is the peak position of the main reflection (1 1 1).

In the case of the cubic structure, only the 4 0 0 reflection is present, while a splitting into separate 4 0 0 and 0 0 4 reflections is expected for the tetragonal phase, indicating $c/a > 1$. However, this splitting is not evident in nanosized $Zr_{0.5}Ce_{0.5}O_2$ powders, because of the very small particle size and the resulting broad XRD peaks. Nevertheless, a marked asymmetry indicative of such splitting is observed in this peak [11–13].

To confirm the tetragonal phase, Raman spectroscopy was used. The tetragonal phase ($P4_2/nmc$ space group) exhibits six Raman-active modes (one A_{1g}, three E_g and two B_{1g} modes), while the

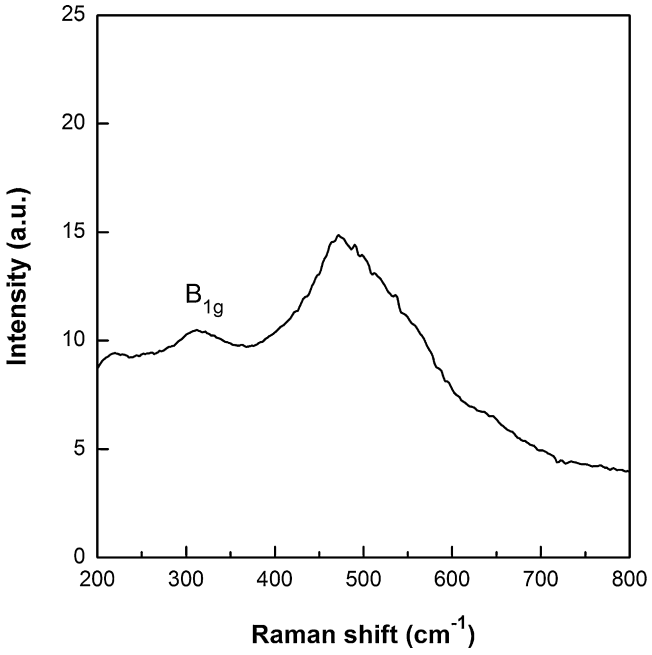

Fig. 3. Raman spectrum obtained for ZC solid solution calcined at 500 °C for 1 h.

cubic phase (*Fm*3*m* space group) only presents one F_{2g} Raman-active mode. In the case of the *t*″ form, it has been reported that some modes of the tetragonal phase are not detected [5]. In Fig. 3, the peak corresponding to the B_{1g} Raman-active mode (312 cm^{-1}) confirms the presence of the tetragonal phase.

A structural study was performed by Rietveld refinement employing the FullProf program [15]. For the tetragonal phase, the $P4_2/nmc$ space group was assumed, with (Zr^{4+}, Ce^{4+}) cations and

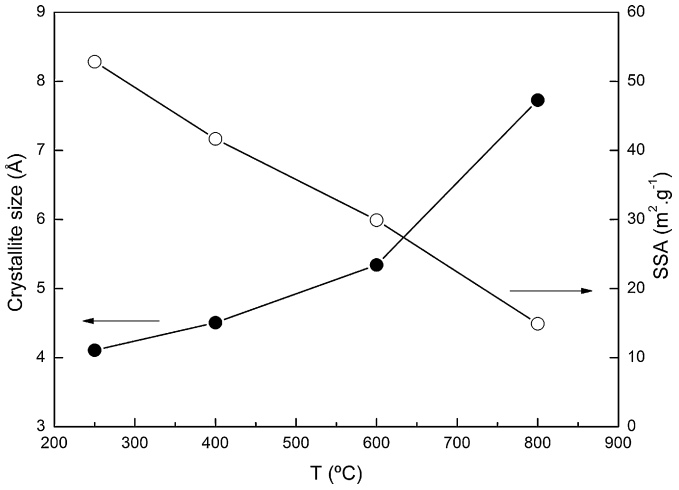

Fig. 4. Crystallite size and SSA values as a function of calcination temperature.

O^{2-} anions in 2a and 4d positions, respectively. The results of these refinements were given in terms of the usual pseudo-fluorite unit cell. The peak shape was assumed to be a pseudo-Voigt function. The background of each profile was fitted using a six-parameter polynomial function in $(2q)^n$, $n = 0–5$. The thermal parameters corresponding to Zr and Ce atoms were assumed to be equal. The results of Rietveld refinements of XRD data for ZC powders calcined at different temperatures are summarized in Table 1. The lattice parameters do not show significant variation between samples treated at different temperatures.

In Fig. 4, crystallite size (determined by the Sherrer formula) and SSA values are represented as a function of calcination temperature. It is clear that as the temperature was increased, the crystallite size increased and the SSA values decreased.

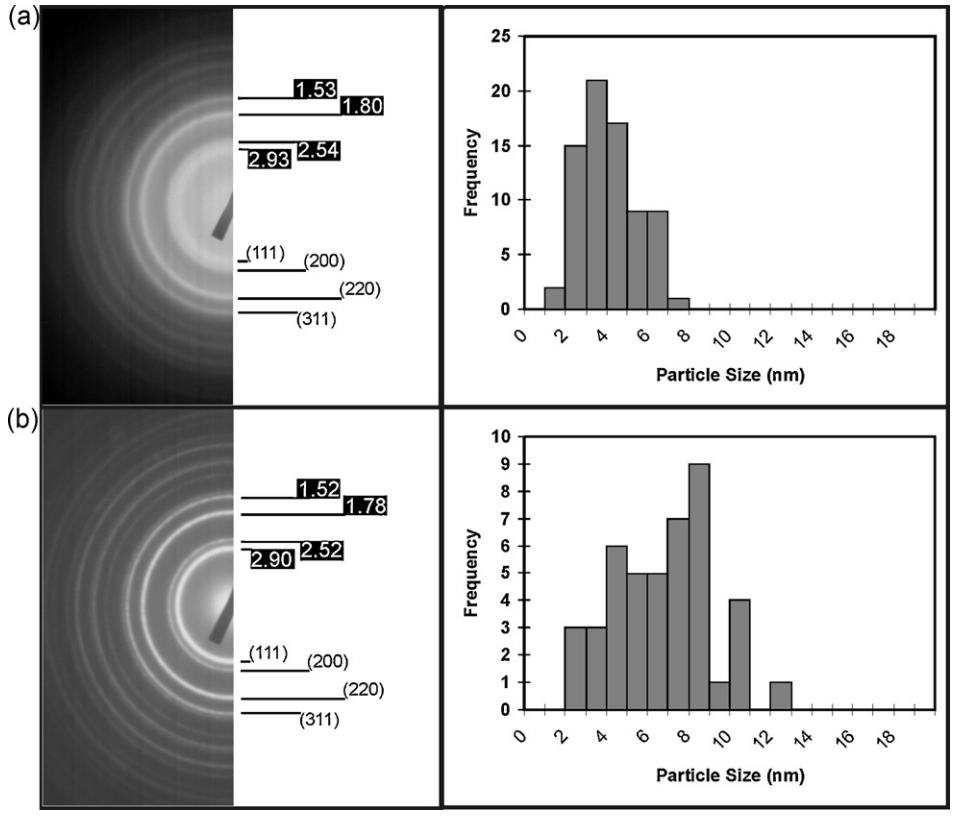

Fig. 5. SAED patterns (left) and histograms of nanoparticle size distribution (right) for ZC samples after calcination for 1 h at (a) 250 °C and (b) 800 °C.

Table 1
Structural parameters and standard Rietveld agreement factors for nanocrystalline ZC solid solutions calcined at different temperatures. For identification purposes, the number in the sample name indicates the calcination temperature in °C. The figure in parenthesis represents standard deviation in the last quoted place.

	ZC250	ZC400	ZC600	ZC800
Space group	$P4_2/nmc$	$P4_2/nmc$	$P4_2/nmc$	$P4_2/nmc$
a (Å)	5.2802(5)	5.2825(7)	5.2830(7)	5.2831(5)
c (Å)	5.299(1)	5.296(2)	5.294(2)	5.295(1)
c/a	1.004(2)	1.003(3)	1.002(1)	1.002(3)
R_p	7.24	7.22	6.91	7.94
R_{wp}	8.52	8.39	8.06	8.82
R_e	6.40	6.42	6.18	6.46
χ^2	1.77	1.71	1.71	1.87

SAED patterns and particle size distribution histograms for the ZC sample after calcination for 1 h at 250 °C and 800 °C are presented in Fig. 5. It should be noted that, even after calcination at only 250 °C, the resulting sample is clearly crystalline. The SAED patterns can all be indexed to the pseudo-Fluorite structure. As calcination temperature was increased, it is seen that average particle size increased also (Fig. 4), and that the particle size distribution became broader, as would be expected. This is also reflected in a corresponding decrease in the width of the diffraction lines in the SAED patterns. The samples calcined at 250 °C and at 800 °C are compared in low, intermediate and high magnification TEM images in Fig. 6. The particles are arranged in sheet-like agglomerations in both samples. The general increase in particle size on increasing calcination temperature is also clear. The high magnification images show the internal structure of a single nanocrystal of each sample. Each nanocrystal is aligned in the [0 1 1] zone axis of

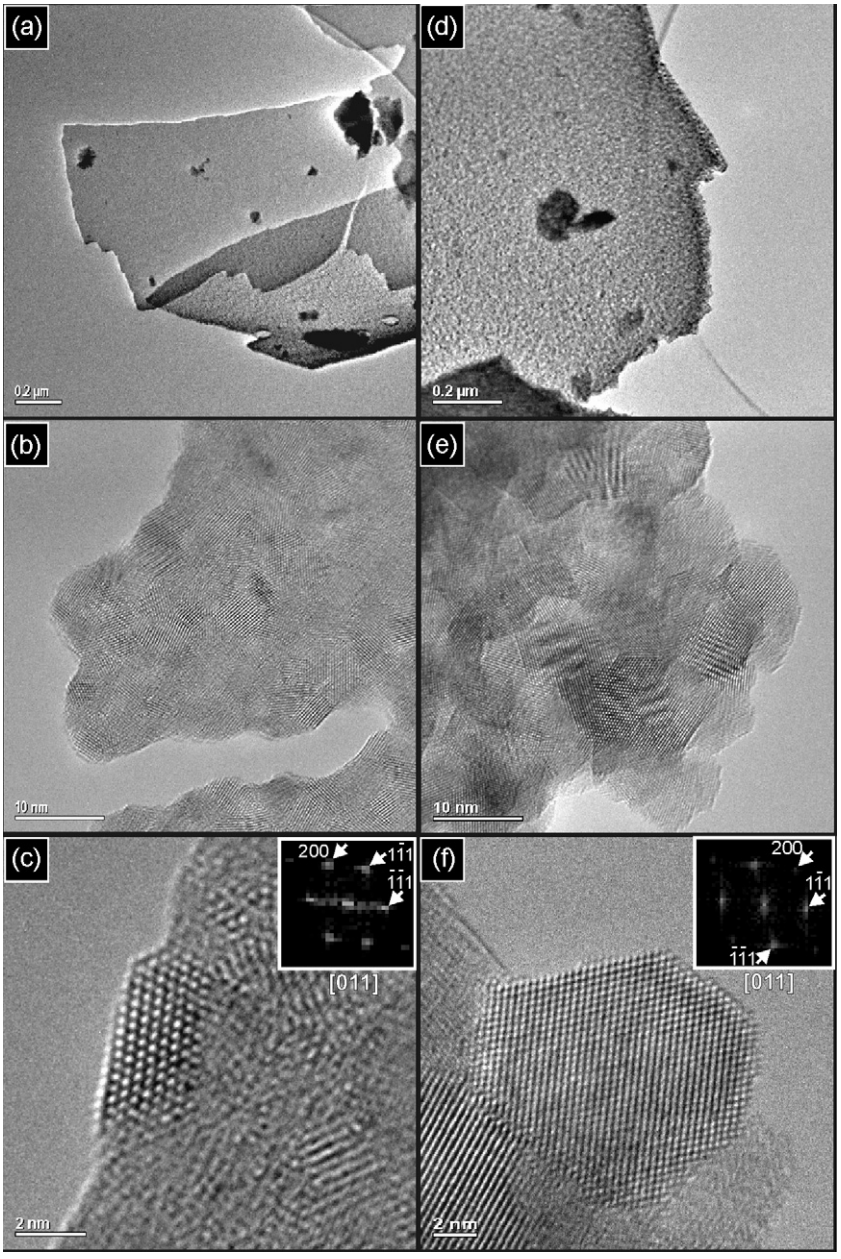

Fig. 6. HRTEM images of ZC250 recorded at (a) low; (b) intermediate; (c) high magnification, and of ZC800 recorded at (d) low; (e) intermediate; (f) high magnification. Both high magnification images show nanocrystals aligned in the [0 1 1] zone axis. DDPs are inset and the diffraction spots are indexed to the fluorite structure.

Table 2
Average crystallite size of ZrO_2–50 mol% CeO_2 powders calcined at 250 °C and 800 °C for 1 h calculated by Scherrer's equation (D_{XRD}), SSA and primary particle size (d_{BET}) and measured from TEM images.

Sample	D_{XRD} (nm)	A ($m^2\ g^{-1}$)	d_{BET} (nm)	d/D ratio	D_{VTEM} (nm)
ZC250	4.1(1)	53(1)	16.0	3.88	5.38
ZC800	7.7(4)	14.9(2)	64.6	8.36	8.99

the pseudo-Fluorite structure, as shown by the digital diffraction patterns (DDPs) inset in each image.

The SAED, TEM and XRD results agree that the sample was crystalline after calcination at only 250 °C. The fact that the DTA shows a significant mass loss between 250 °C and the next calcination temperature, 400 °C, initially seems puzzling, therefore. However, this difference can be explained by the fact that the DTA experiment involves a temperature ramp rate, and so is a transient technique, whereas the calcinations applied to the material prior to study by TEM, XRD and SAED were at constant temperature for a period of 1 h. In transient experiments, peaks occur at slightly higher temperature than they would if the process had taken place isothermally. Therefore, a process that starts at, or slightly above, a certain temperature in DTA would be expected to proceed to a significant extent, and perhaps to completion, at that same temperature when applied isothermally for an extended period. This appears to be the case for the processes related to the crystallization of the CZ by 250 °C in the present study.

In Table 2, results of average crystallite size, BET specific surface area (SSA) and the primary particle size, d_{BET}, calculated from the BET data, are summarized. The average particle size, calculated from the BET data, was estimated by means of the equation: $d_{BET} \sim 6/\rho A$, where ρ is the theoretical density of the material and A is the SSA of the powder. The theoretical density was calculated from XRD results for all the compositions using the formula $\rho \sim ZM/N_A V$, where Z is the number of formula units in the unit cell, M is the formula weight, N_A is Avogadro's number and V is the unit cell volume. The d_{BET}/D_{XRD} ratio in ZC250 sample was less than the ratio for ZC800, indicating that the crystallites of ZC250 exhibited a lesser degree of agglomeration. Values of primary particle size determined by TEM, d_{VTEM}, were found to be consistently slightly higher than the d_{XRD} values. This may be because of a small degree of polycrystallinity in the nanoparticles or may be related to the individual nanocrystals having a disk-like morphology and a preferred orientation with their long axes in the plane of the sheet-like structures seen in Fig. 6a and d.

4. Conclusions

A nanocrystalline ZrO_2–50 mol% CeO_2 solid solution was synthesized by a citrate complexation method. The structural properties of the $Zr_{0.5}Ce_{0.5}O_2$ material calcined at different temperatures were studied by XRD and transmission electron microscopy. Crystallization of the material had occurred after calcination at 250 °C for 1 h. Particle size measurements in TEM agreed well with the estimate obtained from the XRD data using the Scherrer equation. All samples exhibited a tetragonal structure ($P4_2/mnc$ space group) and the lattice parameters were not affected when crystallite size increased.

Acknowledgments

This work was carried out within the UK EPSRC SUPERGEN Fuel Cell consortium (Phase One). Electron microscopy was carried out at the Electron Microscopy Facility, University of St. Andrews.

References

[1] J. Kaspar, P. Fornasiero, N. Graziani, Catal. Today 50 (1999) 285–298.
[2] J. Kaspar, P. Fornasiero, N. Hickey, Catal. Today 77 (2003) 419–449.
[3] S. Bernal, G. Blanco, J.J. Calvino, J.M. Gatica, J.A. Pérez Omil, J.M. Pintado, Top. Catal. 28 (1–4) (2004) 31–46.
[4] J. Kaspar, P. Fornasiero, in: A. Trovarelli (Ed.), Catalysis by Ceria and Related Materials, Imperial College Press, London, 2002 (Chapter 6).
[5] R. Di Monte, J. Kaspar, J. Mater. Chem. 15 (2005) 633–648.
[6] J.R. Gonzalez-Velasco, M.A. Gutierrez-Ortiz, J.L. Marc, J.A. Botas, M.P. Gonzalez-Marcos, G. Blanchard, Appl. Catal. B 22 (1999) 167–172.
[7] S. Rossignol, F. Gerard, D. Duprez, J. Mater. Chem. 9 (1999) 1615–1620.
[8] A. Cabañas, J.A. Darr, E. Lester, M. Poliakoff, J. Mater. Chem. 11 (2001) 561–568.
[9] M. Yashima, K. Ohtake, M. Kakihana, M. Yoshimura, J. Am. Ceram. Soc. 77 (1994) 2773–2776.
[10] J. Kaspar, P. Fornasiero, G. Balducci, R. Di Monte, N. Hickey, V. Sergo, Inorg. Chim. Acta 349 (2003) 217–226.
[11] D.G. Lamas, G.E. Lascalea, R.E. Juárez, E. Djurado, L. Pérez, N.E. Walsöe de Reca, J. Mater. Chem. 13 (2003) 904–910.
[12] D.G. Lamas, R.O. Fuentes, I.O. Fábregas, M.E. Fernández de Rapp, G.E. Lascalea, J.R. Casanova, N.E. Walsöe de Reca, A.F. Craievich, J. Appl. Cryst. 38 (2005) 867–873.
[13] R.O. Fuentes, R.T. Baker, J. Phys. Chem. C 113 (3) (2009) 914–924.
[14] H. Klug, L. Alexander, X-ray Diffraction Procedures for Polycrystalline and Amorphous Materials, John Wiley, New York, 1974, p. 618.
[15] J. Rodríguez-Carvajal, FullProf98, Version 0.2, Laboratoire León Brillouin (CEA-CNRS), Saclay, France, 1998.